


# The thin and medium filters of the EPIC camera on-board XMM-Newton: measured performance after more than 15 years of operation

Marco Barbera<sup>1,2</sup>  • Fabio Gastaldello<sup>3</sup> •  
Luisa Sciortino<sup>1</sup> • Simonpietro Agnello<sup>1</sup> •  
Gianpiero Buscarino<sup>1</sup> • Alfonso Collura<sup>2</sup> •  
Nicola La Palombara<sup>3</sup> • Ugo Lo Cicero<sup>2</sup> •  
Nicola Sartore<sup>3</sup> • Andrea Tiengo<sup>3,4,5</sup> •  
Salvatore Varisco<sup>2</sup> • Anna Maria Venezia<sup>6</sup>

Received: 8 April 2016 / Accepted: 10 July 2016 / Published online: 5 August 2016  
© Springer Science+Business Media Dordrecht 2016

**Abstract** After more than 15 years of operation of the EPIC camera on board the XMM-Newton X-ray observatory, we have reviewed the status of its Thin and Medium filters. We have selected a set of Thin and Medium back-up filters among those still available in the EPIC consortium and have started a program to investigate their status by different laboratory measurements including: UV/VIS transmission, Raman scattering, X-Ray Photoelectron Spectroscopy, and Atomic Force Microscopy. Furthermore, we have investigated the status of the EPIC flight filters by performing an analysis of the optical loading in the PN offset maps to gauge variations in the optical and UV transmission. We both investigated repeated observations of single optically bright targets and performed a statistical analysis of the extent of loading versus visual magnitude at different epochs. We report the results of the

---

✉ Marco Barbera  
marco.barbera@unipa.it

<sup>1</sup> Università degli Studi di Palermo, Dipartimento di Fisica e Chimica, Via Archirafi 36, 90123 Palermo, Italy

<sup>2</sup> Istituto Nazionale di Astrofisica, Osservatorio Astronomico di Palermo, Piazza del Parlamento 1, 90134 Palermo, Italy

<sup>3</sup> Istituto Nazionale di Astrofisica, Istituto di Astrofisica Spaziale e Fisica Cosmica, Via E. Bassini 15, 20133 Milano, Italy

<sup>4</sup> Istituto Universitario di Studi Superiori Pavia, Piazza della Vittoria 15, 27100 Pavia, Italy

<sup>5</sup> Istituto Nazionale di Fisica Nucleare, Sezione di Pavia, via A. Bassi 6, 27100 Pavia, Italy

<sup>6</sup> Consiglio Nazionale delle Ricerche, Istituto per lo Studio dei Materiali Nanostrutturati, Via U. La Malfa 153, 90146 Palermo, Italy

measurements conducted up to now. Most notably, we find no evidence for change in the UV/VIS transmission of the back-up filters in ground tests spanning a 2 year period and we find no evidence for change in the optical transmission of the thin filter of the EPIC-pn camera from 2002 to 2012. We point out some lessons learned for the development and calibration programs of filters for X-ray detectors in future Astronomy missions.

**Keywords** X-rays: XMM-Newton · X-rays: instrumentation · X-rays: filters

## 1 Introduction

The European Photon Imaging Camera (EPIC) on-board XMM-Newton [1] provides focal plane imaging and spectrometry for the three X-ray telescopes. There is one EPIC camera at the focus of each telescope: two cameras contain MOS CCDs [2], while the third camera is based on PN CCDs [3]. All three cameras have an identical forward section that contains a filter wheel, door, calibration source, radiation shielding, the interface to the spacecraft focal plane bulkhead, and the internal bulkhead that forms part of the camera vacuum enclosure.

The filter wheel with its gears and motor is located on the vacuum side of the bulkhead. It has six locations for filters, and six small apertures through which the calibration source can shine onto the CCDs (Fig. 1).

The source itself is mounted on the vacuum side of the bulkhead. The three cameras were fully evacuated when XMM was still on ground, so that at the satellite launch they

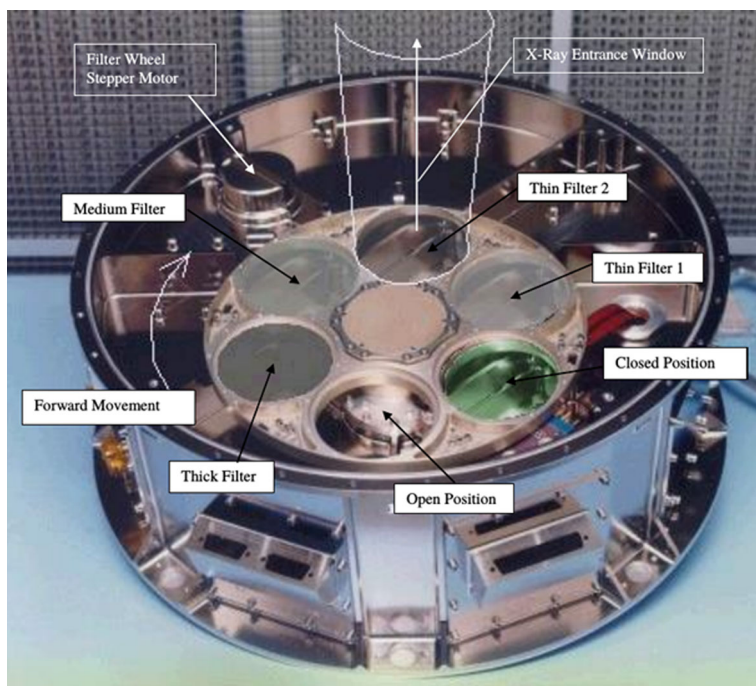


**Fig. 1** Picture of one of the filter wheel of the PN and MOS detectors (from [2])

were in vacuum condition and thus filters did not suffer from significant acoustic load generated by the rocket motors.

Currently the MOS and PN CCDs are operated at  $-120$  and  $-90$  °C, respectively (Kirsch et al. [4], SPIE 5898, 224). Molecules from the outgassing of the spacecraft reaching the cold surface of the CCD could build up a contamination layer affecting the operation of the instrument. The filters, which operate at about  $20$  °C, provide a warm primary barrier to molecules, though the gaps around the filter could allow molecules to reach the CCD surface by several bounces.

The two main categories of contamination are particulate, which has almost energy-independent impacts on the effective area, and molecular contamination, the effects of which are energy dependent. The monitoring of the camera contamination is based on the periodic observation of a set of X-ray sources which are considered photometric and spectrometric standards. They are the isolated neutron star RX J856-3754 and the supernova remnants N132D and 1 E0102.2-7219. The latest measurements show traces of contamination in the MOS2 camera modeled as  $\sim 35$  nm of pure Carbon, and the MOS1 modeled as  $\sim 10$  nm of pure Carbon; on the other hand, the PN camera shows no significant particle or molecular contamination and only upper limits can be given [5]. A more significant amount of Carbon contamination ( $>210$  nm) has been detected so far on the Reflection Grating Spectrometer (RGS) [6]. The time evolution of the thickness of the Carbon contamination layer is well fitted with an exponential model [7]. The contamination on the EPIC detectors is, however, much lower than what found on Chandra and Suzaku [8,9].

No definite explanation has been found yet for the different contamination level between the four EPIC detectors except for possible differences in the external thermal environment. The RGS which has the larger contamination could partially be affected by the lack of optical filters which, in the other three detectors, can partially contribute to block the ballistic propagation of molecules from the spacecraft environment.

Three different filters, can alternatively be used on the filter wheel to prevent optical and UV light from reaching the detectors and to protect the CCD from molecular and particle contamination. The Thin (two for each camera) and Medium filters, developed under the responsibility of the Italian research team in the EPIC consortium [2,10,11], have been manufactured by MOXTEK Inc. and consist of a polyimide membrane  $\sim 160$  nm thick coated with aluminum on one single side, namely  $\sim 40$  nm on the thin filter and  $\sim 80$  nm on the medium filter. The Thick filter, developed at the Max-Planck-Institut für Extraterrestrische Physik (MPE, Germany), consists of a polypropylene membrane  $\sim 350$  nm thick with  $\sim 100$  nm of aluminum on one side and  $\sim 100$  nm of aluminum and  $\sim 25$  nm of tin on the other side [3,12]. The three filters are self-supporting and 76 mm in diameter.

Following the experience gained in the calibration program of the Chandra High Resolution Camera (HRC) UV/Ion shields [13,14], the high energy resolution X-ray transmission curves of one Thin (G18) and one Medium (G19) EPIC filters have been measured at the Berliner Elektronenspeicherring-Gesellschaft für Synchrotronstrahlung (BESSY) (Berlin, Germany) to derive the fine structure features near the absorption edges (XANES and EXAFS) of the atomic elements in the filter material (C, N, O, Al). These measurements have been used to complement the

tabulated imaginary part of the atomic scattering factors [15] in order to derive the transmission model of the EPIC Thin and Medium filters in the full energy range of interest [11].

UV/Vis transmission measurements in the range 190–1000 nm have been performed between May 1997 and July 2002 on one Thin (T4) and one medium (G12) EPIC on-ground qualification filters to monitor their time stability [16]. The filters have been stored in dry Nitrogen between April 1997 and December 1999, and in vacuum, after the launch of XMM-Newton, between January 2000 and July 2002, to follow a story as close as possible to the flight filters. Such measurements have shown an increase in transmission in the first year of the monitoring activity, followed by a stabilization. According to [13] the change in transmission cannot be interpreted simply with an increase of the aluminum oxidation layer. Among possible alternative explanations are: a change in the polyimide structure that reduces the intensity of the characteristic absorption bands at about 250 nm, or an increase in the surface roughness of aluminum that reduces the reflected component.

One of the two monitored back-up filters (G12) was damaged accidentally at the end of the previous monitoring program during a transfer from the vacuum chamber to the UV/VIS spectrophotometer. Fragments of this filter were stored inside a dry-nitrogen cabinet and have been used for the XPS measurements reported below. The thin filter T4 is still stored in a dry nitrogen cabinet.

After more than 15 years of operation, the performances of the EPIC flight filters may have degraded due to oxidation, contamination, irradiation doses, fractures/holes, etc. Such degradation might introduce changes in: (i) UV/VIS transmission with strong impact on sources with bright optical/UV counterparts; (ii) Spatial homogeneity with strong impact on extended sources,

No major failure of the in-flight EPIC filters has been reported to date after more than 15 years of mission operation, but no specific tests have been recently performed in-flight. In addition, no laboratory measurements on spare flight filters have been performed since the results reported in [16] to check the filter performances. For this reason, as part of the activities funded by the Italian Space Agency to support the XMM-Newton operation, we have started an investigation on the status of the Thin and Medium filters which are under the responsibility of the Italian consortium. In this paper we report the results of this activity, in particular, Section 2 is dedicated to the filter selection and storage, Section 3 is dedicated to laboratory measurements on back-up filters, Section 4 is dedicated to investigate the status of the in-flight filters through the analysis of observational data.

The experimental work conducted on spare flight filters is not to be considered as a complementary investigation on the status of the flight filters since they have followed a story which is significantly different from the laboratory samples (e.g. vacuum, contamination, micrometeoroids impact, etc.), while it is an independent check on the aging of Polyimide/Al filter performances, and an evaluation of the potentials of different experimental techniques for the characterization of thin filters which will be very useful in the development and calibration programs of the filters for the X-IFU [17] and WFI [18] detectors on-board the future high energy Astrophysics mission ATHENA.

## 2 Material and investigation methods

### 2.1 Filter manufacturing process

The EPIC Thin and Medium filters manufactured by MOXTEx consist of a thin film of polyimide, with nominal thickness of 160 nm, coated with a single layer of aluminum whose nominal thickness is 40 nm for the Thin and 80 nm for the Medium filters, respectively. The polyimide thin films are produced by spin-coating of a polyamic acid (PAA) solution obtained by dissolving two precursor monomers (an anhydride and an amine) in an organic polar solvent. For the EPIC Thin and Medium filters the two precursors are the Biphenyldianhydride (BPDA) and the p-Phenyldiamine (PDA) (Dupont PI-2610), and the solvent is N-methyl-2-pyrrolidone (NMP) and Propylene Glycol Monomethyl Ether (Dupont T9040 thinner). To convert the PAA into polyimide, the solution is heated up to remove the NMP and to induce the imidization through the evaporation of water molecules. The film thickness is controlled by spin coating parameters, PAA viscosity, and curing temperature [19]. The polyimide thin membrane is attached with epoxy onto a transfer ring and the aluminum is evaporated in a few runs, distributed over 2–3 days, each one depositing a metal layer of about 20 nm thickness.

The EPIC Thin and Medium flight qualified filters have been manufactured during a period of 1 year, from January'96 to January'97. Table 1 lists the full set of flight-qualified filters (Flight Model and Flight Spare) delivered to the EPIC consortium, together with their most relevant parameters. Along with the production of the flight qualified filters, the prototypes and the qualification filters (not included in this list) have been manufactured and tested for the construction of the filter transmission model and to assess the stability in time of the Optical/UV transparency (opacity). Among these qualification filters are T4, G12, G18, and G19 that have been previously mentioned.

### 2.2 Filter selection and storage

From the list in Table 1 we have identified the five remaining flight spare Thin and Medium EPIC filters stored in the laboratories of INAF-IASF-MI and INAF-OAPA, we have collected the MOXTEx documentation, and have visually inspected their integrity. The five filters, stored inside their original shipping containers, namely 4, 7, 15, 23, and 69 are highlighted in Table 1.

We have arbitrarily chosen to start the verification study on the thin filter N. 23 (in the following identified as T23) and the medium filter N. 69 (in the following identified as M69). Figure 2 provides the MOXTEx datasheets of the two filters showing their main characteristics. The EPIC T23 has a measured thickness of polyimide and aluminum of 181.8 nm and 40.1 nm, respectively, and a peak UV transmission of  $1.5 \cdot 10^{-2}$  in the 200–800 nm wavelength range. The same parameters for the medium filter EPIC M69 are: 170.7 nm, 83.4 nm, and  $1.5 \cdot 10^{-4}$ .

A small vacuum chamber has been set-up at the XACT facility of INAF-OAPA [20] to store the two filters during the investigation period. The chamber



**Table 1** List of flight qualified medium and thin EPIC filters

Num.	Type	Thickness (nm)		Production Date	Pinhole area ( $\times 10^{-4}$ mm <sup>2</sup> )	Transmission			
		polyimide	Al			UV/VIS <sup>a</sup>	C K $\alpha$	Fe L $\alpha$	Si K $\alpha$
01	T FM MOS1	181.8	40.6	08/1996	2.7	1.1E-2	0.67	0.75	0.93
02	T FS	181.7	39.1	08/1996	0.51	2.3E-2	0.67	0.77	0.92
03	M FS	170.5	82.5	07/1996	2	1.1E-4	0.47	0.74	0.91
04	M FS	170.5	82.5	07/1996	1.4	9.1E-6	0.49	0.74	0.89
05	M FM MOS2	170.5	82.5	07/1996	4.7	5.4E-5	0.47	0.75	0.90
06	T FS	177.8	41.3	08/1996	0.69	1.1E-2	0.66	0.77	0.95
07	T FS	173.7	39.1	08/1996	0.24	1.2E-2	0.67	0.78	0.91
08	T FS PN	177.8	41.3	08/1996	0.38	1.3E-2	0.66	0.77	0.94
11	T FS PN	172.3	40.6	09/1996	0.12	1.2E-2	0.67	0.78	NA
12	T FM PN	181.8	40.6	08/1996	0.095	1.1E-2	0.66	0.78	0.94
13	T FS	177.8	41.3	08/1996	1.9	1.1E-2	0.67	0.77	0.94
14	T FM MOS1	177.8	40.4	08/1996	0.67	9.6E-3	0.66	0.77	0.96
15	M FS	184.3	83.0	08/1996	0.83	8.4E-5	0.48	0.73	0.90
17	M FS	162.6	83.4	08/1996	1.5	6.9E-5	0.49	0.71	0.89
18	T FS MOS	172.3	40.6	09/1996	0.11	1.2E-2	0.66	0.77	0.92
21	T FM MOS2	177.8	40.4	08/1996	5.1	1.1E-2	0.66	0.76	0.94
23	T FS	181.8	40.1	08/1996	0.94	1.5E-2	0.68	0.75	0.94
24	T FM MOS2	177.9	39.8	07/1996	23	1.3E-2	0.67	0.77	0.95
32	T FS	173.7	40.0	08/1996	0.44	1.2E-2	0.67	0.76	0.92
33	T FS MOS	180.0	38.8	08/1996	0.42	1.3E-2	0.66	0.74	0.93
40	T FM PN	172.3	40.6	09/1996	0	1.1E-2	0.66	0.77	NA
63	M FS	164.7	85.9	10/1996	0.64	1.2E-4	NA	0.74	NA
65	M FM MOS1	164.7	85.9	10/1996	0.31	1.3E-4	NA	0.72	NA
66	M FM PN	170.7	83.4	10/1996	0	1.2E-4	NA	0.75	NA
67	M FS MOS	170.7	83.4	10/1996	0.31	1.2E-4	NA	0.73	NA
68	M FS PN	170.7	83.4	10/1996	0.67	1.7E-4	NA	0.76	NA
69	M FS	170.7	83.4	10/1996	1.2	1.5E-4	NA	0.74	NA

<sup>a</sup> Peak value in the wavelength band 200–800 nm

is evacuated by a scroll pump providing a clean vacuum in the high  $10^{-2}$  mbar range. Figure 3 shows pictures of the vacuum chamber, the vessel to hold the filters inside the vacuum chamber, and the two inspected filters EPIC T23 and EPIC M69. Vacuum and venting procedures are performed very slowly to prevent turbulent motion of residual particles in the chamber to damage the filters. The samples are kept in atmosphere only during the measurement sessions, and transported inside the MOXTEx original shipping containers from/to the different laboratories.



 <div>EPIC ON BOARD XMM OPTICAL / UV FILTER</div>						 <div>EPIC ON BOARD XMM OPTICAL / UV FILTER</div>					
Certificate of Conformance						Certificate of Conformance					
As Built Configuration List						As Built Configuration List					
THIN FILTER NUMBER: 23						MEDIUM FILTER NUMBER: 69					
PROCESS SPECIFICATION						PROCESS SPECIFICATION					
MATERIAL	MEQ.	PART #	LOT #	SPECIFICATION	ACTUAL	MATERIAL	MEQ.	PART #	LOT #	SPECIFICATION	ACTUAL
Polyimide	DuPont	P02510	J774830	1600 Å +/- 10%	1618 Å	Polyimide	DuPont	P02510	J774830	1600 Å +/- 10%	1707 Å
Aluminum	Alfa AESAR	10748	K30025	400 Å +/- 10%	401 Å	Aluminum	Alfa AESAR	10748	K30025	400 Å +/- 10%	404 Å
Thinner	DuPont	T9039	J814602	N/A		Thinner	DuPont	T9039	J814602	N/A	
Epoxy	Epoxy Technology	EPO-TEK 301	A-22688	N/A		Epoxy	Epoxy Technology	EPO-TEK 301	A-22688	N/A	
		B-18668		N/A				B-18668		N/A	
FUNCTIONAL SPECIFICATION						FUNCTIONAL SPECIFICATION					
PARAMETER	EQUIPMENT	SPECIFICATION		ACTUAL		PARAMETER	EQUIPMENT	SPECIFICATION		ACTUAL	
Pinhole Map	VICKERS Microscope @ 100x	< 4.0 mm <sup>2</sup>		9.4x10 <sup>-4</sup> mm <sup>2</sup>		Pinhole Map	VICKERS Microscope @ 100x	< 0.04 mm <sup>2</sup>		1.2x10 <sup>-4</sup> mm <sup>2</sup>	
Vibration Test	LORAL Vibration Facility	XYZ - axis ± 7.3 mm @ 10.0 G max sweep 4 octave/sec		PASS		Vibration Test	LORAL Vibration Facility	XYZ - axis ± 7.3 mm @ 10.0 G max sweep 4 octave/sec		N/R	
Temperature	LORAL Environmental Chamber	-30 °C to +60 °C		PASS		Temperature	LORAL Environmental Chamber	-30 °C to +60 °C		N/R	
UV-visible Transmission	CARY V	min 1x10 <sup>-1</sup>	peak	1.5x10 <sup>-2</sup>		UV-visible Transmission	CARY V	min 1.0x10 <sup>-4</sup>	peak average	1.5 x10 <sup>-4</sup>	
		max 9x10 <sup>-1</sup>	std	3.9x10 <sup>-4</sup>				max 9.0x10 <sup>-1</sup>	std dev	8.1 x10 <sup>-4</sup>	
X-Ray Calibration						X-Ray Calibration					
	MANSON Source	N/A	Carbon Ka	mean	68.07		MANSON Source	N/A	Carbon Ka	mean	N/R
			relative std dev		0.73%				relative std dev		%
		N/A	Iron La	mean	74.93				Iron La	mean	73.85
			relative std dev		1.14%				relative std dev		1.24%
		N/A	Silicon Ka	mean	94.22				Silicon Ka	mean	N/R
			relative std dev		1.04%				relative std dev		%

**Fig. 2** Certificate of conformance issued by MOXTEK for the EPIC flight spare filters N.23 (thin, identified as T23) and N.69 (medium, identified as M69)

## 2.3 Experimental techniques

### 2.3.1 UV/VIS transmission

UV/VIS transmission measurements in the wavelength range 190–900 nm have been performed at the Dipartimento di Fisica e Chimica of the Università degli studi di Palermo (UNIPA-DiFC) using a JASCO V560 double beam spectrophotometer setting the monochromator band width to 10 nm and the scan speed

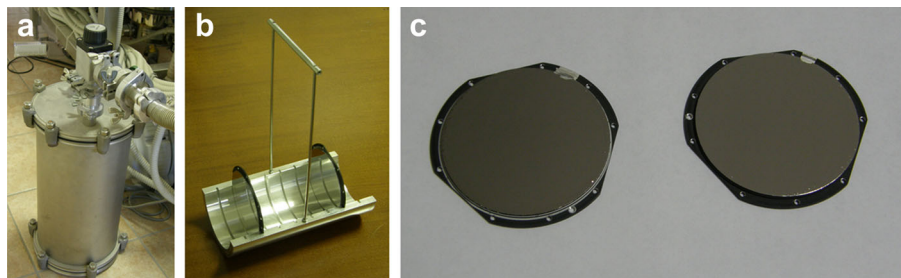


**Fig. 3** Pictures of: the small vacuum chamber set-up at the XACT facility of INAF-OAPA to store the filters under investigation (panel a); the vessel for safe handling of the filters in/out of the chamber (panel b); the two filters on a laminar flow bench (panel c)

to 40 nm/min. The limiting transmission sensitivity of the spectrophotometer with this parameter set-up is in the range  $2\text{--}3 \cdot 10^{-5}$  over the full wavelength range.

### 2.3.2 Raman scattering

Micro-Raman measurements at room temperature were carried out at UNIPA-DiFC using a Bruker-Senterra micro-Raman spectrometer equipped with a 532 nm laser diode excitation. The optimal beam power is derived monitoring the spectra increasing the power from 0.2 to 20 mW. Predictably, a low value of power prevents the acquisition of high quality spectra, while a high value of power damages irreversibly the polyimide. Confocal measurements were done in the range  $50\text{--}4478 \text{ cm}^{-1}$  with a spectral resolution between 9 and  $15 \text{ cm}^{-1}$ . Scans perpendicular to the filter surfaces were also executed to highlight specific spectral features. Furthermore, different points on a given surface were examined in order to evaluate the repeatability of the obtained spectra.

### 2.3.3 Atomic force microscopy

Tapping mode amplitude modulation AFM measurements [21–24] were performed at UNIPA-DiFC by a Multimode V (Veeco Metrology) scanning probe microscope equipped with a conventional piezo-scanner and a four-segment photo-detector for cantilever deflection monitoring. PointProbe®Plus Silicon-SPM-probes were used with aluminum backside reflex coating, resonance frequency about 300 KHz, and tip apical radius 5–10 nm. All the acquired images had a resolution of  $512 \times 512$  pixels, and were obtained with a tip velocity on the surface of about  $2 \mu\text{m/s}$ . Quantitative information on images were extracted using the GWYDDION software.<sup>1</sup>

### 2.3.4 X-ray photoelectron spectroscopy

The X-ray photoelectron spectroscopy (XPS) analyses were performed at Istituto per lo Studio dei Materiali Nanostrutturati - Consiglio Nazionale delle Ricerche in Palermo with a VG Microtech ESCA 3000 Multilab, using the non-monochromatic Al  $K_{\alpha}$  source (1486.6 eV) run at 14 kV and 15 mA. The pass energies of 50 eV and of 20 eV were used in the hemispherical electron energy analyzer for the survey and the individual peak energy regions, respectively. As it is the case for the AFM measurements, the XPS investigation has been performed on small fragments of the G12 EPIC Medium back-up filter. Two samples were mounted with double-sided adhesive tape onto a stainless-steel holder. In one case the membrane was mounted exposing the aluminum side (side up), in another case exposing the polyimide side (side down). Binding energies were referenced to the C 1 s binding energy of adventitious

---

<sup>1</sup> <http://gwyddion.net/> (2010)



carbon set at 285.1 eV. The software provided by VG was used for peak analyses and for the calculation of the atomic concentrations. The precision on the binding energy and on the atomic percentage values was respectively  $\pm 0.15$  eV, and  $\pm 10$  %.

### 3 Ground laboratory measurements

#### 3.1 UV/VIS transmission

UV/VIS transmission measurements in the wavelength range 190–900 nm have been performed every 3 months, from March 2011 to July 2013 (10 measurements). The first measurement session (March 03, 2011) was carried out on filters previously stored inside the MOXTEx boxes. The second session (June 17, 2011) was conducted after the filters were maintained in vacuum for about a month. Since then, filters have been always kept in vacuum.

The measured transmission curves are shown in Fig. 4 together with two sets of measurements performed on similar filters as references, namely T4 (Thin) and G12 (Medium), in September 1997 and July 2002 in a previous monitoring program [16].

All measurements performed on both filters EPIC T23 and EPIC M69 show no evidence for change over the 2 years monitoring time span. The first measurements performed when the filters were still stored in the original MOXTEx boxes show no significant difference from measurements performed after the filters were stored in vacuum.

The measured transmission curves are consistent with the values reported in the MOXTEx datasheet (Fig. 2) and in good agreement with the transmission curves measured in 2002 for G12 and T4 filters. Notice that the measurements performed in 1997 on the same G12 and T4 filters are significantly lower than the other measurements. As briefly mentioned in the introduction, the previous monitoring campaign performed on EPIC filters between 1997 and 2002 has shown a change in transmission after about one and half year while filters were stored in dry

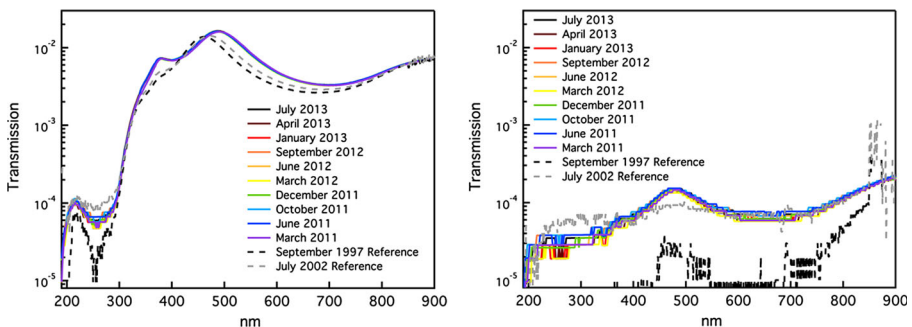


**Fig. 4** UV/VIS transmission curves measured on the EPIC T23 filter (*Thin*, left panel) and EPIC M69 filter (*Medium*, right panel). Superimposed are also the transmission curves measured on similar filters in a previous monitoring program

Nitrogen. The transmission measurements did not present further change between mid 1998 and 2002. The measured change in transmission could not be interpreted simply with an increase of the aluminum oxidation layer [16].

The small shift of the resonance peak at about 450 nm of the EPIC T23 with respect to T4 is due to a slightly different nominal thickness of polyimide for the two compared filters, namely 1818 Å for EPIC T23, and 1656 Å for T4.

### 3.2 Raman scattering

The formation of Al-C and Al-O bonds between a subatomic monolayer of aluminum and the polyimide film has been observed experimentally using the High Resolution Electron Energy Loss (HREEL) technique that induces vibrational bands [25]. Based on this experimental evidence we have decided to investigate the occurrence of interfacial polymer-Al bonds in our filters using the micro-Raman technique.

Both the polyimide and the aluminum side of the filters EPIC T23 and EPIC M69 have been investigated. The measured spectra obtained by illuminating the Al side are dominated by a strong continuum, likely luminescence, which does not allow to detect vibrational signals. The measured Stokes Raman spectra, obtained illuminating the polyimide side of the filters, are shown in Fig. 5.

Although the range of the acquired spectra is large, we show in Fig. 5 only the range 1140–1850  $\text{cm}^{-1}$ , that is the region of interest for polyimide materials. As a reference the Raman signal of a fresh sample of naked polyimide (manufactured in 2013), TF111-519 sample, is recorded. A second-degree polynomial is subtracted from the spectra as background, then the intensity of Raman spectra are normalized to the peak located at 1619  $\text{cm}^{-1}$ . Measurements have a high degree of repeatability. Both the spectrum of the EPIC T23 filter (manufactured in 1996) and the spectrum of the fresh polyimide sample show quite similar features in terms of spectral position and shape of the peaks. Such evidence suggests that the EPIC T23 filter is chemically undamaged. In Fig. 5 several features of a typical polyimide spectra are recognizable [26–28]. The main peak at 1619  $\text{cm}^{-1}$  is ascribable to the vibration  $\nu_{\text{C}=\text{C}}$  and the peaks in the 1700–1800  $\text{cm}^{-1}$  is the carboxyl region where the vibration  $\nu_{\text{C}=\text{O}}$  are found.

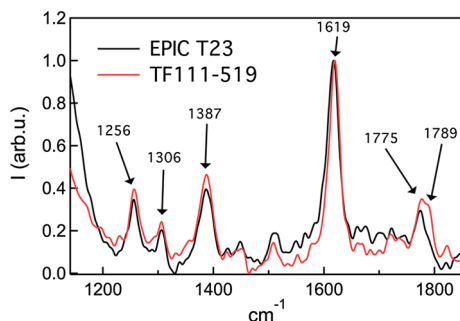


**Fig. 5** Raman spectra of the EPIC T23 compared to a naked polyimide (TF111-519) as reference

### 3.3 Atomic force microscopy

The measurement apparatus does not allow to perform a direct measurement on one of the large format EPIC filters. Furthermore, the risk of damage measuring a free-standing thin filter is high. For this reason we have conducted the AFM investigation on small fragments of the Medium filter G12 that was investigated during the previous aging monitoring program between 1997 and 2002. Two samples of few  $\text{mm}^2$  size have been prepared, one with the aluminum side facing up and the other one with the polyimide side facing up. The sample with polyimide facing up, similarly to EPIC T23 and EPIC M69 filters, shows a slightly yellowish color well distinct from the aluminum side that presents a shining silver color.

Figure 6 shows the 3D images (top panels) and associated typical Z-profiles (bottom panels) of the AFM measurements performed on the two prepared samples. The actual image size is  $2 \times 2 \mu\text{m}^2$ , while the full Z scale is  $\pm 30 \text{ nm}$  for the aluminum and  $\pm 2.5 \text{ nm}$  for the polyimide. The aluminum, which was deposited by evaporation, presents a granular structure with typical size of the particles of few nm. A reliable estimate of the particle size, which takes into account the size of the tip, gives an average diameter of the aluminum particles of  $5 \text{ nm}$  with a statistical variance of the distribution of about  $1 \text{ nm}$ . The polyimide is much smoother than aluminum.

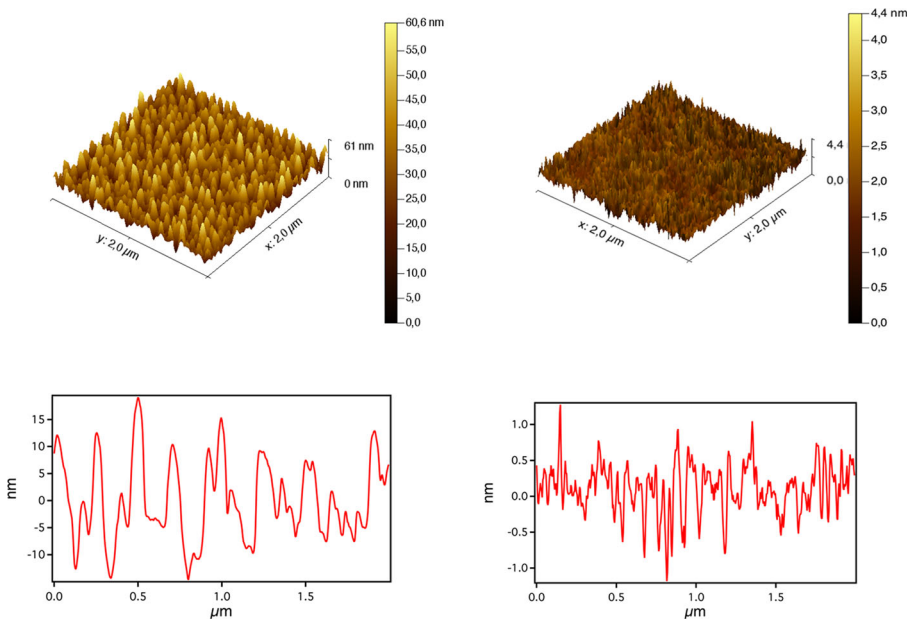


**Fig. 6** 3-D AFM image (*top-left*) of the aluminum side of filter G12. The image has a resolution of  $512 \times 512$  pixels. A typical Z-profile (*bottom-left*) has been measured on the central horizontal line of the AFM image. 3-D AFM image (*top-right*) of the polyimide side of filter G12. A typical Z-profile (*bottom-right*) has been measured on the central horizontal line of the AFM image

### 3.4 X-ray photoelectron spectroscopy

Figure 7 shows the two wide survey scans, characterized by a low energy resolution and high intensity, of the two sides of the filter. The side up (aluminum side) spectrum contains mainly the peaks due to aluminum (Al2p and Al2s), carbon (C1s) and oxygen (O1s and O Auger KLL). Some minor components due to the silicon from the adhesive tape are also present. The side down spectrum contains hardly visible Al peaks and an additional N1s peak at 400.4 eV typical of an imide nitrogen.

Figure 8 shows the experimental Al2p region spectra with the fitted curves of both sample sides. Each spectrum contains the two components, one due to metallic aluminum at 72.7 eV, and the other one due to the amorphous aluminum oxide at 75.5 eV. In the case of the side down sample (lower panel), the intensity of the aluminum peak with the two components is rather low, as it is evident from the larger noise level. In fact, the aluminum which is underneath the polyimide film 160 nm thick is below the information depth of the XPS technique. However, it is likely that attaching the very thin and fragile sample onto the bi-adhesive tape a small fraction of it rolled up, and thus small portions of the aluminum coating are facing-up.

The thickness of the oxide film formed over the aluminum metal was calculated using the formula developed by Strohmeier [29] and Carlson et al.[30] defined as:

$$d = \lambda_{ox} \sin \theta \ln \left[ \frac{N_m \lambda_m I_{ox}}{N_{ox} \lambda_{ox} I_m} + 1 \right] \quad (1)$$

where  $\theta$  is the photoelectron take off angle which in the present instrument configuration is  $90^\circ$ ,  $I_{ox}$  and  $I_m$  are the percentage areas of the oxide and metal peaks,  $N_m$  and  $N_{ox}$  are the volume densities of the metal atoms in the metal and oxide, respectively, and  $\lambda_m$  and  $\lambda_{ox}$  are the electron inelastic mean free path (IMFP) of the metal and oxide, respectively, obtained from the kinetic energies of the photoelectrons according to the algorithm of Penn [31].

Using the formula given above and the measured peak areas of the oxide and metal components, the thickness of the oxide film was estimated as 5.9 nm in both cases. The

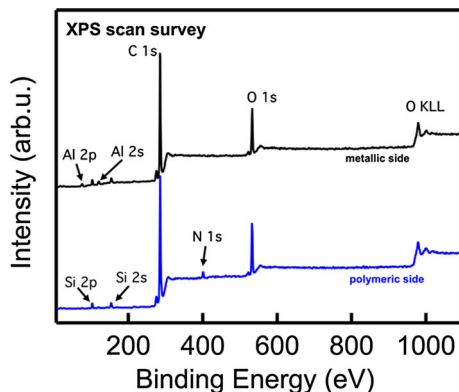


**Fig. 7** XPS Survey scans of the two different sides of the filter sample as reported in the plot

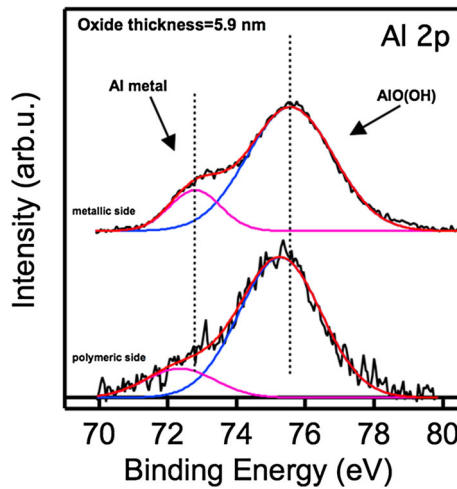


**Fig. 8** XPS scan of the Al 2p binding energy region for the two different sides of the filter sample

survey spectrum of the side down sample contains hardly visible Al peaks and an additional N1s peak at 400.4 eV typical of an imide nitrogen.

#### 4 In flight measurements

The XMM-Newton EPIC CCDs [2,3] are highly sensitive to visible light, therefore if an astronomical target has a high optical-to-X-ray flux ratio the measured signals can be contaminated by optical photons (“optical loading”). To prevent this, the EPIC cameras include three types of aluminized optical blocking filters (thick, medium and thin), and also an internal “Offset Map” which is uploaded before each exposure to subtract the dark-current level of charge or other systematic zero shifts.

Here we report the results on the flight measurements of optical loading in the EPIC-PN offset maps. The analysis of optical loading allows a measurement of the detected optical flux and constrains any variability in the optical transmission which can point to a degradation of the in-flight EPIC filters.

The PN offset maps are uploaded on board at the beginning of each exposure. The offset analysis has been performed following the approach of the instrument calibration team [32,33]: the offset data have been manipulated in order to remove the dominating common mode noise and varying column-to-column gain by subtracting the CCD column and row medians. In the resulting offset maps, so called “residual”, local features such as optical loading due to a star may readily be detected and quantified in terms of residual offset energies, i.e. ADUs relative to the local background, which are then transformed in counts due to optical photons.

For this study we consider the observations taken in Full Frame (FF) mode with the thin filter. To find suitable optical targets with known visual magnitudes, spectral types, and reported variability we cross-correlated the XMM archive with the Hipparcos catalogue and the Bright Star Catalogue [34], that is widely used as a source of basic

astronomical and astrophysical data for stars brighter than magnitude 6.5. These catalogues provide information on magnitude and spectral type. Using these data together with the conversion of residual offset energy to number of detected optical photoelectrons, a comparison of detected optical flux with respect to magnitude can be made. Following an early analysis by the calibration team, we report the peak residual offset, i.e. the maximum residual offset found in the loaded region, and the visual magnitude of the optical loading cases.

We report the results of the analysis performed on a sample of about 200 offset maps with detected optical loading found in thin filter exposures. The results obtained from repeated observations of the same target at different epochs are shown, thus probing directly the possible amount of variation in the optical transmission of the source, and the statistical results based on a possible evolution of the peak residual offset versus visual magnitude relation.

We found many XMM fields with the presence of bright optical stars in the field of view, observed at different times in FF mode with the thin filter. One of the best examples is the field of NGC 5408 that has been repeatedly observed because of the bright Ultra Luminous X-ray source present in the galaxy. Close to the X-ray source there is the star V828 Cen (HD 122532) which is a 6.11 V magnitude variable star of the chemically peculiar type (spectral type B9p) with known optical variability of 3.68 days. In Table 2 we report the main parameters of the various observations. As it can be seen, the deviations from the mean of the peak residual offset (mean = 274 ADU) is consistent with zero over a time span of 8.5 years, and the most deviant point is just 1.5  $\sigma$  away from the mean.

We have collected the results on a sample of 200 offset maps with detected optical loading found in thin filter exposures. Such maps have been divided in two equal size samples to have similar statistics, namely: an early sample, going from revolution 860 to revolution 1421 (from 20/08/2004 to 12/09/2007), and a late sample, from revolution 1422 to revolution 2299 (from 14/09/2007 to 28/06/2012). The peak residual offsets are shown in the right and left panel of Fig. 9 for the early and late samples, respectively, vs. the visual magnitude of the optical counterpart. The best-fit exponential functions are also shown: they are in agreement with the expected theoretical relationship  $A \cdot 10^{(-0.4 M)}$  where M is the visual magnitude. The normalization of the best-fit relation between the two samples differs by only 3 % and this difference is well below the

**Table 2** Parameters of the various observations of the NGC 5408 field, in particular the obsid and revolution of the observations, the off-axis angle of the star in arc-minutes given as output by the SAS task *ecoordconv*

Obsid	Revolution	Obs date	Off-axis (arcmin)	CCD	Peak (ADU)
0112291001	0483	29/07/2002	3.4	1	271 ± 19
0302900101	1117	13/01/2006	2.8	7	265 ± 19
0500750101	1483	13/01/2008	2.8	7	301 ± 20
0653380201	1942	17/07/2010	3.4	1	252 ± 19
0653380301	1943	19/07/2010	3.3	1	259 ± 19
0653380401	2039	26/01/2011	2.6	7	307 ± 20
0653380501	2040	28/01/2011	2.6	7	266 ± 19



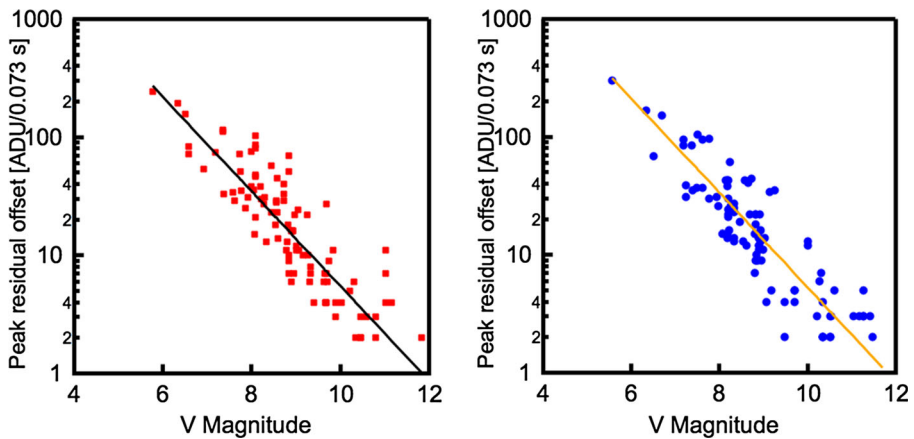


**Fig. 9** Peak residual offset versus visual magnitude for the investigated late sample of PN images with known sources of optical loading (*left panel*), namely from revolution 1422 to revolution 2299 (from September 2007 to June 2012), and for the investigated early sample of PN images (*right panel*) from revolution 860 to revolution 1421 (from August 2004 to September 2007). The drawn line represents the best fit exponential function

intrinsic scatter due to the inclusion of various spectral types (which can also lead to a factor of two difference in optical loading from a M0 star and a B9 star) and observations at different off-axis angles.

In summary, we have investigated the status of the EPIC thin filter performing an analysis of 200 cases of optical loading in the PN offset maps of FF mode observations. We did not find any indication of variability in the optical transmission, both by analyzing repeated observations of the same targets and from a statistical analysis of the relationship between optical loading and visual magnitude of the star responsible for it.

## 5 Summary and conclusions

In this paper we have reported results from an experimental program aimed at investigating the status of the EPIC Thin and Medium filters after more than 15 years of operation of the XMM-Newton observatory in Space, and nearly 20 years from production of the filters by MOXTEx. We have selected two representative filters of Thin and Medium types, flight qualified and stored as spares in the laboratories of the EPIC consortium. The two filters, EPIC T23 and EPIC M69, were initially stored in their original shipping container built by MOXTEx. A small chamber was set-up at the XACT facility of INAF-OAPA to store the two filters in vacuum during the investigation program.

In order to verify the status of the two filters, we have used different experimental techniques, mainly non-destructive, not all of them commonly used in the investigation of thin X-ray filters, but each one potentially capable of providing useful information:

- UV/VIS transmission measurements performed on both EPIC T23 and EPIC M69 show no evidence of change with time during the over 2 years period of monitoring.

The first measurement performed on March 2011, when the filters were still stored in the original MOXTEX containers, are indistinguishable from the other measurements performed after the filters have been stored in vacuum. The measured transmission curves are in good agreement with the transmission curves measured in 2002 for similar filters.

- RAMAN scattering data on the polyimide side of the investigated filters show spectral features typical of the material. The features are present in both filters and are repeatable in different location on the filters. The same features are present in a freshly produced sample of polyimide confirming that the filters have not undergone chemical damage.
- AFM measurements show that the evaporated aluminum is structured in granules with average diameters of 5 nm. Typical linear profiles show a height peak to valley ranging between 10 and 30 nm. These values are of the same order of magnitude as the nominal average thickness of aluminum in the Thin (40 nm) and Medium (80 nm) filters.
- The XPS measurements allow to quantify the thickness of the surface aluminum oxide which turns out to be  $5.9 \text{ nm} \pm 10 \%$ . This result is in good agreement with the aluminum oxide thickness derived previously from the analysis of high resolution X-ray transmission measurements performed with synchrotron light source [35] and UV/Vis absorption measurements [13,16].

Beside the laboratory measurements, performed on back-up flight filters, we have investigated the status of the flight EPIC thin filter by comparison of repeated observations of the same targets and by performing an analysis of 200 cases of optical loading in the PN offset maps of full frame mode observations and investigating the relation between optical loading and visual magnitude of the star responsible for it. We did not find any indication of variability in the optical transmission of the thin filter of the PN CCD. This analysis has been performed only on the PN CCD because its operation mode requires that an offset map is computed before the beginning of each observation, as explained in the text. The analysis of the MOS data for what concerns optical loading is less straightforward. Although this analysis is limited only to the thin filter of the PN CCD, it should be representative, for what concerns filter ageing and contamination, of the performance of the other thin and medium filters which are mounted on the same filter wheel, thus operating at the same temperature and in a similar environment.

The MOS cameras (in particular MOS2) have suffered a position dependent change in the low energy QE, which has been interpreted as due to contaminants which have adhered to the cold surface of the cameras. Such contamination is currently modeled as pure Carbon, similar to that observed on the RGS, and is growing with time at a steady rate of nearly 1 nm/year on the MOS1 and 3 nm/year on the MOS2 [36].

A calibration experiment performed in 2012 observing the thermal SNR 1E0102-72 has shown consistency of the measured spectra, for all cameras and all filters, with the same astrophysical model [37]. The lack of evidence for significant residual discrepancies at the carbon edge confirms that no significant contamination has built up onto the filters.

EPIC has suffered so far four events of micrometeorite impacts. Two of these occurred on MOS1 and have caused its CCD6 (stroke in 2005) and CCD3 (stroke in

2012) to become unusable for Science. The events are interpreted as micrometeorite debris, with typical particle size estimated to be  $< 1 \mu\text{m}$ , scattered off the mirror surface under grazing incidence and reaching the focal plane detector. No major damage on the filters has been recorded after such events, while it is likely that passing through the filters micrometeorites produce small pinholes. Since the filters are located at nearly 15 cm above the focal plane, the focal spot at the filter position is quite large ( $\sim 15 \text{ mm}$  diameter). The ratio between the area of a pinhole and that one of the focal spot is very small ( $< 10^{-8}$ ) and thus it cannot be detected in any type of investigation to be performed in-flight.

In conclusion, the available information from in-flight calibrations and the results obtained on back-up filters stored in laboratory confirm that the Thin and Medium filters built by MOXTEx for the EPIC experiment on-board the XMM-Newton mission are still in good shape after nearly 20 years from production. They are fully compliant with the scientific requirements, and not significantly modified since the previous measurement campaigns. Aluminum coated polyimide filters are robust and reliable in time confirming that such materials are presently still one of the best choice for the filters on future X-ray experiments in Space missions.

**Acknowledgments** We acknowledge financial contributions by the Italian Space Agency through ASI/INAF agreements I/023/05/0 and I/088/06/0 for the data analysis and I/032/10/0 for the XMM-Newton operation. We thank M.J.S. Smith and M. Freyberg for help with the analysis of PN offset maps.

## References

1. Jansen, F., Lumb, D., Altieri, B., Clavel, J., Ehle, M., Erd, C., Gabriel, C., Guainazzi, M., Gondoin, P., Much, R., Munoz, R., Santos, M., Schartel, N., Texier, D., Vacanti, G.: XMM-Newton observatory. I. The spacecraft and operations. *Astron. Astrophys.* **365**, L1–L6 (2001)
2. Turner, M.J.L., et al.: The European photon imaging camera on XMM-Newton: the MOS cameras. *Astron. Astrophys.* **365**, L27–L35 (2001). doi:[10.1051/0004-6361:20000087](https://doi.org/10.1051/0004-6361:20000087)
3. Strüder, L., et al.: The European photon imaging camera on XMM-Newton: the pn-CCD camera. *Astron. Astrophys.* **365**, L18–L26 (2001). doi:[10.1051/0004-6361:20000066](https://doi.org/10.1051/0004-6361:20000066)
4. Kirsch, M.G., Abbey, A., Altieri, B., Baskill, D., Dennerl, K., van Dooren, J., Fauste, J., Freyberg, M.J., Gabriel, C., Haberl, F., Hartmann, H., Hartner, G., Meidinger, N., Metcalfe, L., Olabarri, B., Pollock, A.M., Read, A.M., Rives, S., Sembay, S., Smith, M.J., Stuhlinger, M. and Talavera, A.: Health and cleanliness of the XMM-Newton science payload since launch, *Proc. SPIE*, Vol. 5898, pp. 224–235 (2005)
5. Sembay, S., Saxton, R.: EPIC-MOS contamination parameters, XMM-Newton, CCF Release Note, XMM-CCF-REL-305 (2013)
6. González-Riestra, R.: Status of the RGS calibration, XMM-newton calibration technical note XMM-SOC-CAL-TN-0030 issue 7.4 (2015)
7. Pollock, A.M.T.: The RGS effective area incorporating exponential contamination and a mechanism for rectification, XMM-Newton CCF Release Note XMM-CCF-REL-262 (2010)
8. O'Dell, S.L., Swartz, D.A., Plucinsky, P.P., Freeman, M.A., Markevitch, M.L., Vikhlinin, A.A., Chen, K.C., Giordano, R.J., Knollenberg, P.J., Morris, P.A., Tran, H., Tice, N.W., Anderson, S.K.: Modeling contamination migration on the Chandra X-ray observatory. *Proc. SPIE* **5898**, 313–324 (2005)
9. O'Dell, S.L., Swartz, D.A., Tice, N.W., Plucinsky, P.P., Grant, C.E., Marshall, H.L., Vikhlinin, A., Tennant, A.F.: Modeling contamination migration on the Chandra X-ray observatory II. *Proc. SPIE* **8859**, 88590F (2013). **12 pp**
10. La Palombara, N., Musso, C., Conte, M., Barbera, M.: The filters for EPIC: optimized design. *Astrophys. Space Sci.* **239**, 281–296 (1996). doi:[10.1007/BF00645782](https://doi.org/10.1007/BF00645782)

11. Villa, G.E., Barbera, M., Collura, A., La Palombara, N., Musso, C., Serio, S., Stillwell, R., Tognon, P., Turner, C.: The optical/UV filters for the EPIC experiment. *IEEE Trans. Nucl. Sci.* **45**(3), 921–926 (1998). doi:[10.1109/23.682670](https://doi.org/10.1109/23.682670)
12. Stephan, K.: Optical filters for the EPIC CCD camera on board the XMM astronomy satellite. *Proc. SPIE* **3114**, 166–173 (1997). doi:[10.1117/12.283766](https://doi.org/10.1117/12.283766)
13. Barbera, M., Collura, A., Dara, A., Leone, M., Powell, F.R., Serio, S., Varisco, S., Zombeck, M.V.: Effects of interference and oxidation on the UV/visible rejection properties of filters for soft X-ray detectors. *Exp. Astron.* **7**(1), 51–63 (1997). doi:[10.1023/A:1007919005280](https://doi.org/10.1023/A:1007919005280)
14. Meehan, G.R., Murray, S.S., Zombeck, M.V., Kraft, R.P., Kobayashi, K., Chappell, J.H., Kenter, A.T., Barbera, M., Collura, A., Serio, S.: Calibration of the UV/ion shields for the AXAF High-resolution camera. *Proc. SPIE* **3114**, 74–100 (1997)
15. Henke, B.L., Gullikson, E.M., Davis, J.C.: X-ray interactions: photoabsorption, scattering, transmission, and reflection at  $E = 50\text{--}30,000$  eV,  $Z = 1\text{--}92$ . *At. Data Nucl. Data Tables* **54**(2), 181–342 (1993). doi:[10.1006/adnd.1993.1013](https://doi.org/10.1006/adnd.1993.1013)
16. Barbera, M., Collura, A., Artale, A., Varisco, S., Peres, G., Sciortino, S., Serio, S., Villa, G.E.: Monitoring the stability of thin and medium back-up filters of the XMM-Newton EPIC camera. *Proc. SPIE* **4851**, 264–269 (2003). doi:[10.1117/12.461592](https://doi.org/10.1117/12.461592)
17. Barbera, M., Collura, A., Gatti, F., Lo Cicero, U., Macculi, C., Piro, L., Renotte, E., Sciortino, S.: Baseline design of the thermal blocking filters for the X-IFU detector on board ATHENA, *Proc. SPIE*, 9144, 9144-5U, 11 pp (2014)
18. Barbera, M., Branduardi-Raymont, G., Collura, A., Comastri, A., Eder, J., Kamiński, T., Lo Cicero, U., Meidinger, N., Mineo, T., Molendi, S., Parodi, G., Pilch, A., Piro, L., Rataj, M., Rauw, G., Sciortino, L., Sciortino, S., Wawer, P.: The optical blocking filter for the ATHENA Wide Field Imager: ongoing activities towards the conceptual design, *Proc. SPIE*, 9601, in press (2015)
19. Diahm, S., Locatelli, M.L., Khazaka, R.: BPDA-PDA polyimide: synthesis, characterizations, aging and semiconductor device passivation. In: Abadie, M.J.M. (ed.) *High Performance Polymers: Polyimides Based - From Chemistry to Applications*. (2012). doi:[10.5772/53994](https://doi.org/10.5772/53994)
20. Barbera, M., Candia, R., Collura, A., Di Cicca, G., Pellicciari, C., Sciortino, S., Varisco, S.: The Palermo XACT facility: a new 35 m long soft x-ray beam-line for the development and calibration of next-generation x-ray observatories. *Proc. SPIE* **6266**, 3F (2006). doi:[10.1117/12.673004](https://doi.org/10.1117/12.673004)
21. Binning, G., Quate, C.F., Gerber, C.: Atomic force microscope. *Phys. Rev. Lett.* **56**, 930 (1986). doi:[10.1103/PhysRevLett.56.930](https://doi.org/10.1103/PhysRevLett.56.930)
22. Garcia, R., Perez, R.: Dynamic atomic force microscopy methods. *Surf. Sci. Rep.* **47**, 197–301 (2002)
23. Giessibl, F.J.: Advances in atomic force microscopy. *Rev. Mod. Phys.* **75**, 949–983 (2003). doi:[10.1103/RevModPhys.75.949](https://doi.org/10.1103/RevModPhys.75.949)
24. Seo, Y., Jhe, W.: Atomic force microscopy and spectroscopy. *Rep. Prog. Phys.* **71**, 016101 (2008). doi:[10.1088/0034-4885/71/1/016101](https://doi.org/10.1088/0034-4885/71/1/016101)
25. Pireaux, J.J., Vermeersch, M., Grégoire, C., Thiry, P.A., Caudano, R., Clarke, T.C.: The aluminum-polyimide interface: an electron-induced vibrational spectroscopy approach. *J. Chem. Phys.* **88**, 3353 (1988). doi:[10.1002/\(SICI\)1521-3927\(19981201\)19:12<619::AID-MARC619>3.0.CO;2-](https://doi.org/10.1002/(SICI)1521-3927(19981201)19:12<619::AID-MARC619>3.0.CO;2-)
26. Ge, J.J., Xue, G., Li, F., McCreight, K.W., Wang, S.-Y., Harris, F.W., Cheng, S.Z.D., Zhuang, X., Hong, S.-C., Shen, Y.R.: Surface studies of polyimide thin films via surface-enhanced Raman scattering and second harmonic generation. *Macromol. Rapid Commun.* **19**, 619–623 (1998). doi:[10.1002/\(SICI\)1521-3927\(19981201\)19:12<619::AID-MARC619>3.0.CO;2-Z](https://doi.org/10.1002/(SICI)1521-3927(19981201)19:12<619::AID-MARC619>3.0.CO;2-Z)
27. Gu, X.J.: Raman spectroscopy and the effects of ultraviolet irradiation on polyimide film. *Appl. Phys. Lett.* **62**(13), 1568–1570 (1993). doi:[10.1063/1.108643](https://doi.org/10.1063/1.108643)
28. LaFemina, J.P., Arjavalasingam, G., Hougham, G.: Electronic structure and ultraviolet absorption spectrum of polyimide. *J. Chem. Phys.* **90**, 5154–5160 (1989). doi:[10.1063/1.456558](https://doi.org/10.1063/1.456558)
29. Strohmeier, B.R.: An ESCA method for determining the oxide thickness on aluminum alloys. *Surf. Interface Anal.* **15**, 51–56 (1990). doi:[10.1002/sia.740150109](https://doi.org/10.1002/sia.740150109)
30. Carlson, T.A., McGuire, G.E.: Study of the x-ray photoelectron spectrum of tungsten-tungsten oxide as a function of thickness of the surface oxide layer. *J. Electron. Spectrosc. Relat. Phenom.* **1**(2), 161–168 (1972/1973). doi:[10.1016/0368-2048\(72\)80029-X](https://doi.org/10.1016/0368-2048(72)80029-X)
31. Penn, D.R.: Electron mean-free-path calculations using a model dielectric function. *Phys. Rev. B* **35**, 482 (1987). doi:[10.1103/PhysRevB.35.482](https://doi.org/10.1103/PhysRevB.35.482)
32. Smith, M.: PN Optical Loading. XMM-SOC-CAL-TN-0051. <http://xmm2.esac.esa.int/docs/documents/CAL-TN-0051-1-2.ps> (2008)
33. Smith, M.: PN X-ray Loading. XMM-SOC-CAL-TN-0050. <http://xmm2.esac.esa.int/docs/documents/CAL-TN-0050-1-1.ps> (2013)

34. Hoffleit, D., Warren, W. H. Jr.: Bright Star Catalogue, 5th Revised Ed. (Hoffleit+, 1991). VizieR Online Data Catalog 5050, 0 (1995)
35. Barbera, M., Collura, A., Dara, A.: Calibration of the AXAF-HRC UV/Ion shields at Osservatorio Astronomico di Palermo G.S.Vaiana: III - Synchrotron measurements of XANES in aluminum coated Lexan film samples, pp. 120–133. Proc. SPIE, 2808, (1996)
36. Sembay, S., Saxton, R.: EPIC-MOS contamination parameters, XMM-Newton CCF Release Note XMM-CCF-REL-305 (2013)
37. Smith, M.: EPIC Status of Calibration and Data Analysis. XMM-SOC-CAL-TN-0018. <http://xmm2.esac.esa.int/docs/documents/CAL-TN-0018.pdf> (2015)